submitted to *Oxidation of Metals*, Jan. 2003

The Oxidation Behavior of Y_2O_3-Dispersed β-NiAl

B. A. Pint† and L. W. Hobbs
H. H. Uhlig Corrosion Laboratory
Massachusetts Institute of Technology
Cambridge, MA 02139

†present address:
Oak Ridge National Laboratory,
P. O. Box 2008,
Oak Ridge, TN 37831-6156

Abstract

Y_2O_3-dispersed NiAl was produced by a powder metallurgy process. By adding Y as an oxide dispersion, problems with NiY_x formation and internal oxidation were avoided. Short-term isothermal and cyclic oxidation performance at 1200°-1500°C was compared to cast NiAl with and without Zr. Results indicate that the Y_2O_3 addition was beneficial to scale adhesion and significantly modified the α-Al_2O_3 scale microstructure, similar to a Zr alloy addition. However, at 1400°C and 1500°C, neither the Y_2O_3 or Zr additions changed the scale growth rate, eliminated the formation of voids at the metal-scale interface or prevented scale spallation. These similarities in performance suggest that similar mechanisms occur when the reactive element is added as either an oxide dispersion or an alloy addition.

Keywords: Nickel aluminides, high temperature oxidation, oxide dispersion, reactive element, Al_2O_3 scale

Introduction

Similar to the addition of carbon to iron, a small (<0.5at%) addition of oxygen-active or "reactive" element (e.g. Y, Zr, Ce, Hf) to chromia- and alumina-forming high temperature alloys has a tremendous effect on oxidation behavior.[1-4] This effect has been widely studied for more than 60 years but the debate continues about a mechanistic explanation for their effect. In Ni-base alumina-forming alloys, studying the effect of Y on oxidation behavior is complicated by the formation of Ni_xY precipitates.[5,6] Attempts

at Y doping using surface treatments, such as oxide coatings[7] or ion implantation,[8-11] have not been successful in reproducing the full reactive element (RE) effect, like that observed with alloy additions. For alumina-formers, it has been suggested that a continuous flux of RE ions diffusing from the metal to the metal-scale interface and then to the alumina grain boundaries is necessary to achieve the beneficial RE effects.[4,11] Therefore, uniformly dispersed bulk additions (i.e. alloy additions or oxide dispersions) are required to achieve the RE effect in alumina-forming alloys.

Using a powder metallurgy technique, a model alumina-forming alloy was produced using a Y_2O_3 addition in a β-NiAl matrix. Because of its high aluminum content, β-NiAl is a primary alumina former with virtually no nickel oxide formation and its oxidation behavior has been widely studied.[12-26] Adding Y as an oxide dispersion (OD) eliminated the problem of NiY_x formation due to the low solubility of Y in NiAl and resulted in a more uniform distribution of Y in the alloy. Unlike surface treatments, the addition of an oxide dispersion can provide a continuous supply of Y ions to the growing scale. With an oxide addition, it also is easy to control the type and amount of dopant addition in order to quantify RE effects.[22]

This Y_2O_3-dispersed β-NiAl material has been the subject of papers reporting its microstructure,[23] the effect of the Y_2O_3 dispersion on the θ- to α-Al_2O_3 phase transformation,[24] and its cyclic oxidation behavior at 1200°C.[22] The focus of this paper is the isothermal and cyclic oxidation performance at higher temperatures (1200-1500°C) compared to cast NiAl, with and without a Zr alloy addition. The Y_2O_3 addition in NiAl produced behavior very similar to that of the Zr alloy addition in terms of scale growth rate, scale adhesion and scale microstructure. At 1400°-1500°C, neither type of RE addition was able to sustain an adherent alumina scale, possibly due to an inherent limit in this metal-oxide system.

Experimental Procedure

Gas-atomized β-NiAl (49at%Al) powder was mechanically blended with 1 vol% Y_2O_3 powder in a N_2 atmosphere using a high-speed attritor and steel balls. The powder was then canned and degassed, followed by extrusion at 1232°C. The chemical composition after extrusion is given in Table

I. Characterization of the microstructure has been reported elsewhere.[23] The average grain size was 1-2 μm. Because NiAl is relatively hard and brittle, most of the oxide particles were found on alloy grain boundaries, not within the grains as is commonly observed when a more ductile alloy is milled. The high oxygen content of the material (Table I) was due to the powder metallurgy processing and correlated with the observation, using scanning transmission electron microscopy with x-ray energy dispersive spectroscopy (STEM/XEDS), of large (1 μm), predominantly Al_2O_3 particles in the alloy.[23] Few voids were observed in the metal. For comparison, cast NiAl, undoped and with 0.11at%Zr, also were analyzed, Table I. An alloy containing 0.04 at%Zr was made by extruding powder using the same conditions as for OD NiAl. Without the high energy powder blending step, this material had a much lower O content, Table I.

Oxidation coupons (≈12mm diameter x 1mm thick) were polished to a 0.3μm alumina finish and ultrasonically cleaned in acetone and methanol prior to oxidation. Oxidation experiments were conducted at 1200°C-1500°C in dry, flowing O_2. Specimens were rapidly inserted and removed from a hot furnace for both isothermal and cyclic oxidation. Mass changes were measured continuously using a Cahn model 1000 microbalance to measure the isothermal kinetics and to check for isothermal spallation during cyclic tests. Mass gains were corrected for the evaporation of the Pt-Rh hangdown wire. Specimen mass changes were measured before and after oxidation using a Mettler model AE163 balance. The cycle time at temperature was 2h at 1200°C, 1h at 1400°C and 0.2h at 1500°C in order to grow more comparable oxide thicknesses at each temperature. After oxidation, samples were examined using scanning electron microscopy with x-ray energy dispersive spectroscopy (SEM/XEDS).

Results

1200°C

Figure 1 shows the isothermal oxidation kinetics for OD NiAl compared to undoped NiAl and NiAl+0.11%Zr. At this and higher temperatures, only α-Al_2O_3 scales were formed, except at very short exposures.[24] The lower parabolic rate constant for OD NiAl compared to undoped NiAl (Table II) was attributed to a change in the growth mechanism, as has been demonstrated for NiAl+0.11%Zr using

^{18}O/SIMS experiments.[19] When doped with a RE, α-Al_2O_3 scales grow predominantly by grain boundary diffusion of oxygen. Undoped α-Al_2O_3 grows faster because both Al and O boundary transport contribute to the mass transport. The similar growth rate for Zr- and Y-doping suggests that both scales grew by the same mechanism. Previous work[25,26] has detected the segregation of Zr and Y ions on the α-Al_2O_3 grain boundaries in each respective case. For example, the average x-ray intensity ratio[25] on the grain boundaries near the gas interface after 16h at 1200°C was 0.053 Y/Al for OD NiAl, 0.124 Zr/Al for NiAl+0.11%Zr and 0.128 Zr/Al for NiAl+0.04%Zr.

In cyclic testing, OD NiAl showed no scale spallation and similar mass gains as NiAl doped with 0.04%Zr and 0.11%Zr, Figure 2. Undoped NiAl showed mass losses after the first few cycles. Thus, the Y_2O_3 addition was effective in improving short-term alumina scale adhesion. In the same test, Y-implanted NiAl was not able to maintain an adherent scale after 20, 2h cycles.[9]

As has been discussed elsewhere,[24] an RE addition also changes the nature of the scale ridges at the gas interface. Rather than the intrinsic ridges formed on undoped α-Al_2O_3 as a result of Al outward diffusion (Figure 3a), extrinsic ridges on RE-doped α-Al_2O_3 form due to the slower θ to α phase transformation.[20] An example of extrinsic ridges on NiAl+0.11%Zr is shown in Figure 3b after 50h at 1200°C. While it is difficult to compare extrinsic ridges because they may vary due to the underlying NiAl orientation,[14] in general, the ridges were far less distinct on OD NiAl after 50h, Figure 3c. However, after 200h, the ridges were somewhat more distinct, Figure 3d. The lack of ridges after 50h is attributed to the more rapid transformation to an α-Al_2O_3 scale on the oxide dispersed alloy.[24] Their development after 200h possibly reflects a small amount of Al outward transport during growth of the scale. To put the size of the ridges in perspective, fracture cross-sections of the alumina scale after 50h are shown in Figure 4. The ridges make up only a small fraction of the total oxide thickness, suggesting that Al transport represents only a minor contribution. With either Y_2O_3 (Figure 4a) or Zr (Figure 4b), the alumina scale had a very similar, columnar microstructure with some grains extending over the entire scale thickness. Again, this microstructure was attributed to growth primarily by grain boundary transport of oxygen and a preferred growth direction. Recent x-ray diffraction work on α-Al_2O_3 formed on ODS FeCrAl has identified the direction as a ≈20° tilt off of (104).[27] This type of columnar

microstructure has been widely observed on RE-doped alumina scales[3,22,23,28] and confirms that the Y_2O_3 dispersion produced all of the typical RE benefits at 1200°C.

1400°C

The oxidation behavior was explored at higher temperatures in order to accelerate the scale growth rate and to determine the relative efficacy of RE additions at higher temperatures. Previous work suggested that RE additions become much less effective in improving oxidation performance at temperatures over 1300°C.[4,29-35] Lifetime modeling has suggested that the addition of Zr to NiAl extends the maximum operating temperature by only 50°C because of excess spallation at higher temperatures.[35]

Figure 5 shows the isothermal kinetic data at 1400°C. The Y_2O_3 addition showed no reduction in the oxidation rate at this temperature, with parabolic rate constants to those for undoped NiAl, Table II. The addition of 0.04%Zr also showed little effect on the oxidation rate. However, NiAl+0.11%Zr showed accelerated attack under these conditions with the formation of blue-green Ni-rich oxide.[30] OD NiAl was run to 100h with no similar effect.

After a 50h isothermal exposure at 1400°C, the scale formed on undoped NiAl was generally 15-20μm thick and flaked off in large sheets. Some spallation also was observed with Zr additions. For OD NiAl, the scale initially was adherent upon removal from the furnace. However, within 1h at room temperature the scale experienced an explosive failure where virtually all of the scale spalled.

Based on the behavior after isothermal exposures, it was not surprising that these alloys spalled in cyclic testing, Figure 6. After the first few cycles, undoped NiAl spalled uniformly after each cycle with a nearly linear mass loss (as has been modeled[35]). The RE-doped alloys showed better behavior initially but eventually began to spall. In two separate tests, OD NiAl spalled a large amount of its scale after the 16th, 1h cycle. The Zr-doped alloys showed a more gradual, but steady mass loss. In one test, NiAl+0.11%Zr showed a higher mass gain but this was attributed to Ni-rich oxide formation, not to a more adherent scale.

Because of the spallation problems after longer exposures, the scale microstructures were compared after 1h at 1400°C, Figure 7. In this case, the α-Al_2O_3 formed on undoped NiAl showed a

clearly different morphology, a seemingly porous oxide, Figure 7a. This structure was attributed to a more significant fraction of growth by outward Al boundary diffusion. It appeared that at this temperature the growth was so rapid that little lateral diffusion occurred near the gas interface to fill in the interior of the grains. The result was large voids at the center of the grains, which eventually sealed off providing a slightly more dense structure shown elsewhere.[36] The scales formed on RE-doped NiAl after 1h at 1400°C had a denser appearance (Figures 7b-7d). In each case, a more typical scale morphology was observed with smaller grains at the gas interface. The smaller grain size may have prevented the large pores from forming within the grains but also allowed more pathways for diffusion.

When spallation was observed on undoped NiAl, the exposed metal was generally smooth with very few grain imprints[12] indicating that there was very little contact remaining between metal and oxide. Oxide growth can still continue with a gap between the metal and scale due to the high Al vapor pressure[13] but, on cooling, the unattached scale spalled in large flakes from the substrate. In the case of OD NiAl, no spallation was observed after the 1h exposure. After 20, 1h cycles, spallation to bare metal was observed, Figure 8a. In this case, there was still a large fraction of grain imprints but there also were some very large, deep voids. Some spallation was observed on NiAl+0.11%Zr after 1h. In the spalled regions, Figure 8b, a larger fraction of voids was observed on the exposed metal surface but these localized areas may have been atypical, otherwise more widespread spallation would have been expected.

The RE-doped scale had a columnar grain structure on both OD NiAl after 1h (Figure 8c) and on NiAl+0.11%Zr after 10h at 1400°C (Figure 8d). The microstructure after 10h gave no indication of the rapid attack observed at longer times (Figure 5). Compared to the grain structure at 1200°C, however, the grain diameters were much larger at 1400°C indicating more grain growth at the higher temperature.

<u>1500°C</u>

The results at 1500°C were similar to those observed at 1400°C. Again, additions of Y_2O_3 and 0.04%Zr showed little effect on the parabolic rate constant (Table II) relative to undoped NiAl, Figure 9. The addition of 0.11%Zr again caused accelerated mass gains associated with the formation of Ni-rich oxide (primarily $NiAl_2O_4$). Using a 0.2h (12min) cycle time, the RE-doped aluminides showed less mass loss in cyclic testing than undoped NiAl, but the beneficial effect was short-lived, Figure 10. After 20

cycles, all of the specimens were losing mass at a similar rate.

The effect of the RE dopants on the scale morphology also became less distinct. Figure 11 shows plan views of the gas interface after 0.2h at 1500°C. The undoped scale (Figure 11a) appeared similar to the scale formed at 1400°C (Figure 7a) with wide ridges and deep recesses between. However, the scales formed on the other alloys showed similar traits, particularly the scales formed on the Zr-doped alloys (Figures 11c and 11d). The numerous small particles on the surface in Figure 11d were identified as ZrO_2. The scale on OD NiAl (Figure 11b) exhibited somewhat finer ridges and fewer deep recesses in the center of grains. Figure 12 shows a cross-section of the scale in Figure 11b. While there was a somewhat columnar grain structure, the grain diameters were much larger than at lower temperatures.

After 20, 0.2h cycles, the spalled regions were examined and only bare metal was observed, indicating spallation on cooling. On OD NiAl, there was a large number of deep voids (Figure 13a) which limited contact between the scale and substrate and likely contributed to the scale spallation. At higher magnification (Figure 13b), both shallow and deep voids were observed but there were few large defects. Surrounding the voids were grain imprints indicating good contact between substrate and scale. Some areas showed outward metal protrusions (arrows by #1) while in other locations it appeared that the protrusions had sheared off during spallation (arrows near #2). This would appear to indicate very good adhesion at the interface, On NiAl+0.04Zr, large shallow voids were observed in the spalled regions, Figure 13c. Some of the voids showed terraced morphologies (arrows) which typically form as Al evaporates from the surface at temperature. The areas between voids showed grain imprints and outward metal protrusions as in Figure 13b.

At longer times at 1500°C, more spallation occurred from all of the alloys making characterization of the scale morphology more difficult. The scales on undoped NiAl and Zr-doped NiAl spalled in large flakes after 50h. However, the scale on OD NiAl initially was adherent on cooling and then spalled explosively into tiny pieces within a short time. To avoid this problem, scales were grown isothermally for 4h. In this case, the plan view morphologies appeared to be coarser versions of those observed after 0.2h. The distinctive feature with both Zr- and Y-doping was the increase in volume of RE-rich particles at the gas interface, Figure 14. For the scale formed on OD NiAl (Figure 14a), the

particles were YAl_xO_y. For NiAl+0.11%Zr, the particles are ZrO_2 and appear to sit on top of the alumina scale, more so than the Y-rich particles, possibly as a result of a higher surface energy between ZrO_2 and Al_2O_3. The ZrO_2 particle size and density as a function of time were quantified using SEM image analysis in a separate study[37] which showed that the volume and size of the ZrO_2 particles increased with oxidation time but the volume was independent of alloy Zr content.

Discussion

The goal of this work was to produce a model alloy for the study of the RE effect. To a large degree that goal was achieved. Compared to previous work on RE coatings[7] or RE ion implantation,[8-10] this Y_2O_3 dispersion produced the full range of RE effects of improved scale adhesion, reduced α-A_2O_3 growth rate and modified scale microstructure. The result is not surprising since the same effect has been found in FeCrAl where Y_2O_3 (e.g. Special Metals MA956, Plansee PM2000 and Dour Metal ODM751) and ZrO_2 (e.g. Kanthal APM) dispersions[3,38-41] produce alloys with excellent oxidation resistance, comparable to RE alloy additions. The one area of concern is that the current OD NiAl contained a very high oxide content (Table I) which may have produced some negative effect on oxidation performance. Producing the alloy in a more controlled environment could result in a lower oxygen content and possibly better performance.

In fact, better performance was the unstated goal of this work. Previous studies on oxide dispersions in NiCrAl[42], CoCrAl[43,44] and Fe_3Al[45,46] have suggested that oxide dispersions might provide superior performance to an alloy addition by avoiding internal oxidation. However, that was not found in this study. A Y_2O_3 addition in NiAl may be expected to outperform a Y alloy addition which is likely to have problems with NiY_x formation and associated internal oxidation.[5] But, when the effects of a Y_2O_3 addition were compared to those of a more soluble RE dopant, like Zr, their performance was similar over the times and temperature ranges investigated here. One hope was that the Y_2O_3 dispersion would improve performance at higher temperatures compared to Zr doping. While OD NiAl did not exhibit accelerated oxidation at higher temperatures like NiAl+0.11%Zr (Figures 5 and 9), scale spallation still occurred. Since the accelerated attack was mitigated by reducing the Zr content in the

alloy, it is possible that this phenomenon is related to excessive internal oxidation of Zr. Incorporation of ZrO_2 particles within the scale would facilitate rapid oxygen transport which could lead to accelerated attack. It also has been suggested that internal oxidation contributes to scale spallation due to the RE-rich oxide particle acting as a stress concentrator.[5] However, similar spallation was noted for all of the RE-doped NiAl alloys even though internal oxidation should not occur with a Y_2O_3 addition.

Considering the large temperature drop on cooling, it also is possible that for oxides formed at 1400° and 1500°C that the cooling-induced strains associated with the expansion mismatch between NiAl and a relatively thick Al_2O_3 scale exceed the interfacial strength and/or the oxide strength. Cooling stresses are a function of the temperature drop (ΔT) and the difference in thermal expansion between substrate and scale ($\Delta\alpha$).[47] Thermal expansion measurements of NiAl show its instantaneous expansion increasing more rapidly above 1200°C[48] which would mean that both terms are increasing, making the critical scale thickness for failure decrease more rapidly with increasing temperature. This intrinsic limitation to lower temperatures and thinner scales fits with the observations that all of the scales failed at higher temperatures. However, the scale on OD NiAl failed explosively after cooling, unlike the other alloys. The area fraction of interfacial voids observed on failure of OD NiAl (Figures 8a and 13a) may have been sufficient to cause spallation but the shearing off of metal protrusions (Figure 13b) suggests a strong interface, despite the failure. While the void formation in OD NiAl did not necessarily cause failure at 1400° and 1500°C, it has been linked to increased scale spallation at long times (>500h) at 1200°C.[49] The formation of interfacial voids in oxide-dispersed NiAl alloys has been discussed previously[22] and may result from factors such as entrapped gas in the metal or coalescence of voids in the as-processed material. However, small voids were not observed in TEM characterization of the as-processed alloy.[23]

There is still some question as to how a RE oxide dispersion provides the same benefit as a RE alloy addition or whether the two types of additions work by the same mechanism. This issue is addressed by the dynamic segregation theory (DST).[4] The outward diffusion of RE ions from the substrate to the gas interface is the basis for the RE effect where an outward flux of RE ions dopes the metal-oxide interface and the α-Al_2O_3 grain boundaries. The nucleation and growth of RE-rich particles

at the gas interface is the hallmark of this mechanism. As is clear from Figure 14, the outward diffusion occurs whether the RE is added as an oxide dispersion (Y_2O_3) or an alloy addition (Zr). The Y_2O_3 particles in the substrate are not neutral actors. According to the DST, during oxidation, Y is drawn by the oxygen potential gradient to leave the oxide particles (e.g., increasing the value of x with time in the compound YAl_xO_y) and becomes segregated to the metal-scale interface and incorporated into the scale. While the amount of RE incorporated into the scale appears to be reduced if the RE is added as an oxide compared to an elemental addition,[37] the fundamental mechanism is the same. Previously proposed explanations for the beneficial effect of oxide dispersions such as gettering S to the dispersoid-matrix interface or the dispersoids acting as a vacancy sinks[6] were not confirmed experimentally.[3-4] Also, if the Y-rich oxide particles in the scale were simply the result of incorporation as the metal was consumed, they should not become concentrated at the gas interface. The increase in particle volume at the gas interface[37] (compare Figures 11b,11d,14a and 14d) indicates that RE oxide particles are not passive participants.

Not only does the RE improvement with scale adhesion diminish with temperature but this also is the case for the reduction in scale growth rate[3,9,15,22] associated with the change in scale growth mechanism.[19,39] The DST suggests that the change in rate is due to the slow outward diffusion of RE ions blocking the normal outward diffusion of Al ions which normally contribute to the growth of undoped α-Al_2O_3 scales. Previously, it has been confirmed that RE ions segregate to grain boundaries in alumina scales from 1000°C-1500°C.[25] However, at the higher temperatures, it is possible that the relative importance of cation transport or grain boundary transport becomes less important to the growth of the scale. For example, if grain boundary transport of oxygen becomes the predominant growth mechanism of undoped Al_2O_3, then RE-doping would not alter the rate by slowing cation transport. There are no unambiguous data comparing the temperature dependence of Al and O boundary diffusion rates over this temperature range. However, the ridge morphology at the gas interface of undoped Al_2O_3 (Figure 7a) at 1400°C suggests that outward Al boundary transport plays a significant role in the early stages (1h) of oxidation at this temperature. At longer times when the oxide grains are much larger, there may be an increased contribution of lattice transport which also would preclude any benefit of RE grain

boundary segregants.

Another explanation for the reduced RE effect with temperature is that the RE ions diffuse more rapidly at higher temperatures, thus having less of an effect on the cation boundary transport. This hypothesis is supported by the observation that the volume of RE-rich particles at the gas interface increases strongly with temperature.[4,25,37] Another factor to consider is that large cation segregants on oxide grain boundaries slow grain growth by a solute drag effect and this effect diminishes with increasing temperature.[50] Comparing the scales formed on OD NiAl at 1200°C (Figure 4a) and 1500°C (Figure 12), it is clear that the grain diameters have increased significantly. Thus, the RE segregants are not able to maintain a small grain size at higher temperatures which also suggests that they may have less of an effect on diffusion in the oxide. While the grain size of RE-doped scales increased with temperature, an undoped scale also underwent more grain growth and appeared to have an even larger grain size with correspondingly fewer diffusion paths. Based on grain imprints in the metal, the grain size on OD NiAl after 50h at 1400°C was 2-3μm, while the grain size of the scale on undoped NiAl was ≈10μm.[29] This would provide at least an order of magnitude larger grain boundary volume in the RE-doped scale. Thus, RE-doping could still inhibit Al boundary transport at 1400°C but, due to the increased diffusion pathways in the finer grained scale, the scale growth rate would not be reduced relative to an undoped scale. At 1500°C, the RE dopants did not significantly change the scale microstructure (Figure 11) thus it is not surprising that little change in the growth rate was observed. A similar oxide appeared to form in each case.

Because of the expense of fabrication and the intrinsic brittleness of β-NiAl, it is unlikely that OD NiAl has any significant commercial application. Experience from fabricating this material indicated that NiAl was too brittle to achieve a nanometer-scale dispersion during mechanical blending (thus making oxide dispersions ineffective in improving the poor mechanical properties of β-NiAl[51-52]). However, in the case of Y_2O_3, the dispersion in these materials appeared sufficient to achieve an improvement in oxidation resistance. Future work with model oxide dispersed NiAl alloys may provide additional insight into the role of reactive elements and, particularly, into optimizing these important benefits.

Summary

β-NiAl with a 1 vol.% addition of Y_2O_3 was oxidized in short-term isothermal and cyclic tests at 1200°, 1400° and 1500°C. Its performance was compared to undoped NiAl and Zr-alloyed NiAl. In these tests, the Y_2O_3 addition showed similar improvements in scale adhesion as a Zr alloy addition. Both reactive element additions are more effective at 1200°C than at 1400° or 1500°C. During 1200°C testing, the addition of Y_2O_3 or Zr to NiAl reduced the scale growth rate and eliminated scale spallation. Examination of the scale morphologies formed at 1200°C showed a columnar α-Al_2O_3 scale formed on Y_2O_3-dispersed NiAl typical of Zr-alloyed NiAl and other reactive element doped alumina-formers. At higher temperatures, the dopants were less effective, inducing little change in the scale growth rate and less pronounced changes in the scale microstructure. At both 1400° and 1500°C, the improvement in scale adhesion with the addition of Y_2O_3 or Zr was short-lived. This may be an intrinsic limitation of the thermal expansion mismatch of NiAl and Al_2O_3 or may be due to the formation of interfacial voids during oxidation. Neither Y_2O_3 or Zr prevented the formation of interfacial voids at these higher temperatures. These similarities in performance suggest that the same mechanisms were active when the reactive element was added as either an oxide dispersion or an alloy addition.

Acknowledgments

The authors are very grateful to the Electric Power Research Institute for providing financial support, Dr. R. Mason and Prof. N. J. Grant for assistance with powder blending, Homogeneous Metals, Clayville, NY for the NiAl powder, and Dr. J. D. Whittenberger and Dr. J. Doychak at NASA Lewis for extruding the OD NiAl alloy and providing the NiAl ingots. P. F. Tortorelli and I. G. Wright provided useful comments on the manuscript at ORNL.

References

1. D. P. Whittle and J. Stringer, *Philosophical Transactions of the Royal Society of London*, Serial A **295**, 309-29 (1980).
2. A. Strawbridge and P. Y. Hou, *Materials at High Temperature* **12**, 177-81 (1994).
3. B. A. Pint, A. J. Garratt-Reed and L. W. Hobbs, *Materials at High Temperature* **13**, 3-16 (1995).
4. B. A. Pint, *Oxidation of Metals* **45**, 1-36 (1996).
5. J. D. Kuenzly and D. L. Douglass, *Oxidation of Metals* **8**, 139-78 (1974).
6. A. Kumar, M. Nasrallah and D. L. Douglass, *Oxidation of Metals* **8**, 227-63 (1974).
7. P. Y. Hou, Z. R. Shui, G. Y. Chuang and J. Stringer, *J. Electrochem. Soc.* **139**, 1119-26 (1992).
8. W. J. Quadakkers, J. Jedlinski, K. Schmidt, M. Krasovec, G. Borchardt and H. Nickel, *Appl. Surf. Sci.* **47**, 261 (1991).
9. B. A. Pint and L. W. Hobbs, *J. Electrochem. Soc.* **141**, 2443-53 (1994).
10. E. Schumann, *Oxidation of Metals* **43**, 157-72 (1995).
11. B. A. Pint, *MRS Bulletin* **19** (10), 26-30 (1994).
12. J. L. Smialek, *Metallurgical Transactions* **9A**, 309-20 (1978).
13. H. M. Hindam and W. W. Smeltzer, *J. Electrochem. Soc.* **127**, 1630-35 (1980).
14. T. Homma, H. Hindam, Y. Pyun and W. W. Smeltzer, *Oxidation of Metals* **17**, 223-33 (1982).
15. J. Doychak, J. L. Smialek and C. A. Barrett, in *Oxidation of High-Temperature Intermetallics*, T. Grobstein and J. Doychak eds. (TMS, Warrendale, PA, 1988) p.41-55.
16. J. Doychak, J. L. Smialek and T. E. Mitchell, *Metallurgical Transactions* **20A**, 499-518 (1989).
17. G. C. Rybicki and J. L. Smialek, *Oxidation of Metals* **31**, 275 (1989).
18. M. W. Brumm and H. J. Grabke, *Corrosion Science* **34**, 547-61 (1993).
19. B. A. Pint, J. R. Martin and L. W. Hobbs, *Oxidation of Metals* **39**, 167-95 (1993).
20. J. Doychak, in *Intermetallic Compounds*, Vol.1: Principles, J. H. Westbrook and R. L. Fleischer eds. (John Wiley & Sons, New York, NY 1994) p.977-1016.
21. R. Prescott, D. F. Mitchell, M. J. Graham and J. Doychak, *Corrosion Science* **37**, 1341-64 (1995).
22. B. A. Pint, *Oxidation of Metals* **49**, 531-60 (1998).
23. B. A. Pint, A. J. Garratt-Reed and L. W. Hobbs, *Oxidation of Metals* **56**, 121-47 (2001).
24. B. A. Pint, M. Treska and L. W. Hobbs, *Oxidation of Metals* **47**, 1-20 (1997).
25. B. A. Pint, A. J. Garratt-Reed and L. W. Hobbs, *J. Amer. Ceram. Soc.* **81**, 305-14 (1998).
26. B. A. Pint and L. W. Hobbs, in *High Temperature Ordered Intermetallics VI*, Symp. Proc. v.364, J. Horton, S. Hanada, I. Baker, R. D. Noebe and D. Schwartz, eds. (MRS, Pittsburgh, PA, 1995) p.987-92.
27. M. Lance, unpublished research, ORNL, Oak Ridge, TN, 1998.
28. F. A. Golightly, F. H. Stott and G. C. Wood, *J. Electrochem. Soc.* **126**, 1035-42 (1979).
29. B. A. Pint, Ph.D. Thesis, (Massachusetts Institute of Technology, Cambridge, MA, 1992).
30. B. A. Pint, A. J. Garratt-Reed and L. W. Hobbs, in *Microscopy of Oxidation 2*, S. B. Newcomb and M. J. Bennett eds. (Institute of Metals, London, U.K., 1993) p.463-75.
31. B. A. Pint, A. J. Garratt-Reed and L. W. Hobbs, Journal de Physique IV **3**, C9-247-55 (1993).
32. B. A. Pint and L. W. Hobbs, Electrochem. Soc. Extended Abstracts **93-2**, 676-7 (1993).
33. B. A. Pint and L. W. Hobbs, *Oxid. Met.* **41**, 203-33 (1994).
34. J. Doychak, C. A. Barrett and J. L. Smialek, in *Corrosion & Particle Erosion at High Temperature*, V. Srinivasan and K. Vedula eds.,(TMS, Warrendale, PA, 1989) p.487-514.
35. J. A. Nesbitt and C. E. Lowell, in *High Temperature Ordered Intermetallics V*, Symp. Proc. v.288, I. Baker, R. Darolia, J. D. Whittenberger and M. H. Yoo, Eds. (MRS, Pittsburgh, PA, 1993) p.107-

18.
36. B. A. Pint, *Oxidation of Metals* **48**, 303-28 (1997).
37. B. A. Pint, K. B. Alexander, O. R. Monteiro and I. G. Brown, in *Diffusion Mechanisms in Crystalline Materials*, Symp. Proc. v.527, Y. Mishin, G. Vogl, N. Cowern, R. Catlow and D. Farkas, Eds. (MRS, Pittsburgh, PA, 1998) p.497-502.
38. T. A. Ramanarayanan, M. Raghavan, and R. Petkovic-Luton, *Journal of the Electrochemical Society* **131**, 923-31 (1984).
39. W. J. Quadakkers, H. Holzbrecher, K. G. Briefs and H. Beske, *Oxid. Met*. **32**, 67-88 (1989).
40. M. J. Bennett, H. Romary and J. B. Price, in *Heat Resistant Materials*, K. Natesan and D. J. Tillack, eds. (ASM, Materials Park, OH, 1991) p.95-103.
41. D. Clemens, K. Bongartz, W. Speier, R. J. Hussey and W. J. Quadakkers, *Fresenius' Journal of Analytical Chemistry* **346**, 318-22 (1993).
42. K. L. Luthra and E. L. Hall, *Oxidation of Metals* **26**, 385-96 (1986).
43. D. P. Whittle, M. E. El Dahshan and J. Stringer, *Corrosion Science* **17**, 879-91 (1977)
44. J. Stringer, I. M. Allam and D. P. Whittle, *Thin Solid Films* **45**, 377-84 (1977)
45. B. A. Pint, P. F. Tortorelli and I. G. Wright, *Werkstoffe und Korrosion* **47**, 663-74 (1996).
46. I. G. Wright, B. A. Pint, and P. F. Tortorelli, *Oxidation of Metals* **55**, 333-57 (2001).
47. H. E. Evans, *Materials at High Temperature* **12**, 219-27 (1994).
48. J. A. Haynes, B. A. Pint, W. D. Porter and I. G. Wright, submitted to *Mater. High Temp.* (2001).
49. B. A. Pint and J. L. Smialek, manuscript being prepared for submission to *Oxidation of Metals*,
50. W. D. Kingery, *Solid State Ionics* **12**, 299-307 (1984).
51. A. U. Seybolt, *Trans. ASM* **59**, 860-75 (1966).
52. J. D. Whittenberger, E. Arzt and M. J. Luton, *J. Mater. Res.* **5**, 271-7 (1990).

List of Figures

Figure 1. Isothermal oxidation kinetics at 1200°C. The rates are similar for an alloy addition of Zr and the Y_2O_3 addition. Both are lower than that measured for undoped NiAl.

Figure 2. Specimen mass changes during 2h cycles at 1200°C. The three RE-doped alloys showed no scale spallation while mass losses were noted for undoped NiAl.

Figure 3. SEM secondary electron plan view images of the scale formed at 1200°C on (a) undoped NiAl after 50h, (b) NiAl+0.11at%Zr after 50h, (c) OD NiAl after 50h and (d) OD NiAl after 200h. The ridges vary from grain to grain (b) but become more distinct on OD NiAl with time, (c) and (d).

Figure 4. SEM secondary electron cross-sectional images of the scale formed after 50h at 1200°C on (a) OD NiAl and (b) NiAl+0.04at%Zr. Both exhibit a columnar grain structure.

Figure 5. Isothermal oxidation kinetics at 1400°C. At this temperature, the addition of 0.04%Zr or Y_2O_3 has little positive effect. A 0.11at%Zr addition accelerated the oxidation rate compared to undoped NiAl.

Figure 6. Specimen mass changes during 1h cycles at 1400°C. The three RE-doped alloys showed less mass loss than undoped NiAl, but all had spalled after 20 cycles.

Figure 7. SEM secondary electron plan view images of the scale formed after 1h at 1400°C on (a) undoped NiAl, (b) OD NiAl (c) NiAl+0.04at%Zr and (d) NiAl+0.11at%Zr.

Figure 8. SEM images comparing the metal exposed by scale spallation at 1400°C on (a) OD NiAl after 20, 1h cycles and (b) NiAl+0.11%Zr after 1h and the scale cross-section at the specimen on (c) OD NiAl after 1h and (d) NiAl+0.11%Zr after 10h at 1400°C.

Figure 9. Isothermal oxidation kinetics at 1500°C. Similar to 1400°C, the higher Zr content resulted in accelerated alumina formation.

Figure 10. Specimen mass changes during 0.2h cycles at 1500°C. The three RE-doped alloys showed nearly identical behavior with only marginally better scale adhesion than undoped NiAl.

Figure 11. SEM secondary electron plan view images of the scale formed after 0.2h at 1500°C on (a) undoped NiAl, (b) OD NiAl (c) NiAl+0.04at%Zr and (d) NiAl+0.11at%Zr.

Figure 12. SEM secondary electron image of the specimen edge showing the scale cross-section formed on OD NiAl after 0.2h at 1500°C.

Figure 13. SEM secondary electron plan view images of the metal exposed by scale spallation after 20, 0.2h cycles on (a) and (b) OD NiAl and (c) NiAl+0.04%Zr. Deeper voids were observed in (a) and at higher magnification in (b) on OD NiAl. In (b), #1 arrows mark metal protrusions and #2 arrows mark sheared protrusions. Larger but shallower voids which showed terracing (arrows) were observed in (c).

Figure 14. SEM secondary electron plan view images of the scale formed after 4h at 1500°C on (a) OD NiAl and (b) NiAl+0.11at%Zr. The ZrO_2 particles (b) are more prominent than the YAl_xO_y particles (a).

Table I. Chemical composition of the commercial NiAl alloys (in atomic %) obtained by inductively coupled plasma analysis.

NiAl Alloys	Cast NiAl	Cast NiAl	Extruded NiAl	OD NiAl
Doping:	Undoped	+Zr	+Zr	$+Y_2O_3$
Ni	49.74	49.62	50.04	48.91
Al	50.19	49.78	49.65	48.13
Fe	< 0.01	0.02	0.02	0.02
Cr	< 0.01	< 0.01	< 0.01	0.03
Si	< 0.01	0.03	0.21	< 0.01
Ti			< 0.01	< 0.01
Cu		0.36		
Y	N/A		< 0.01	0.**24**
Zr	N/A	**0.11**	**0.04**	< 0.01
C	0.071	0.071	0.019	0.008
O			0.020	2.66
S	0.0027	0.0027	0.0047	0.0050

Table II. Parabolic rate constants (g^2/cm^4s) of the various NiAl alloys at 1200°-1500°C.

Temperature:	1200°C	1400°C	1500°C
Alloy:			
Undoped NiAl	12-13 x 10^{-12}	5.4-5.9 x 10^{-11}	1.8-1.9 x 10^{-11}
OD NiAl (Y2O3 dispersed)	3.6-4.5	4.6-6.7	2.9-3.5
NiAl+0.04%Zr	2.4-2.7	3.0-4.6	2.7-3.3
NiAl+0.11%Zr	3.3-4.7	12-45*	8.5*

* accelerated attack, non-parabolic behavior

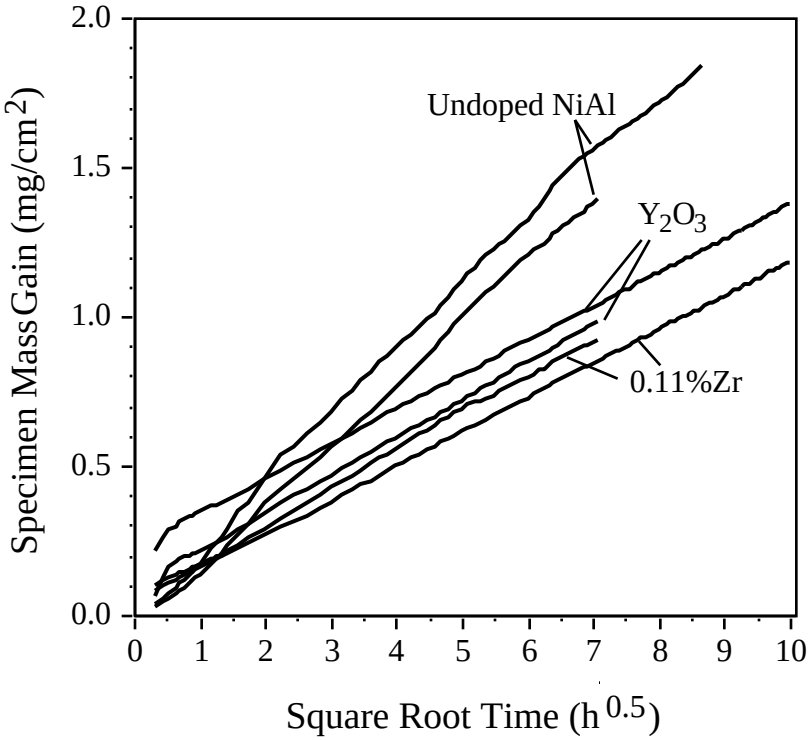

Figure 1. Isothermal oxidation kinetics at 1200°C. The rates are similar for an alloy addition of Zr and the Y_2O_3 addition. Both are lower than that measured for undoped NiAl.

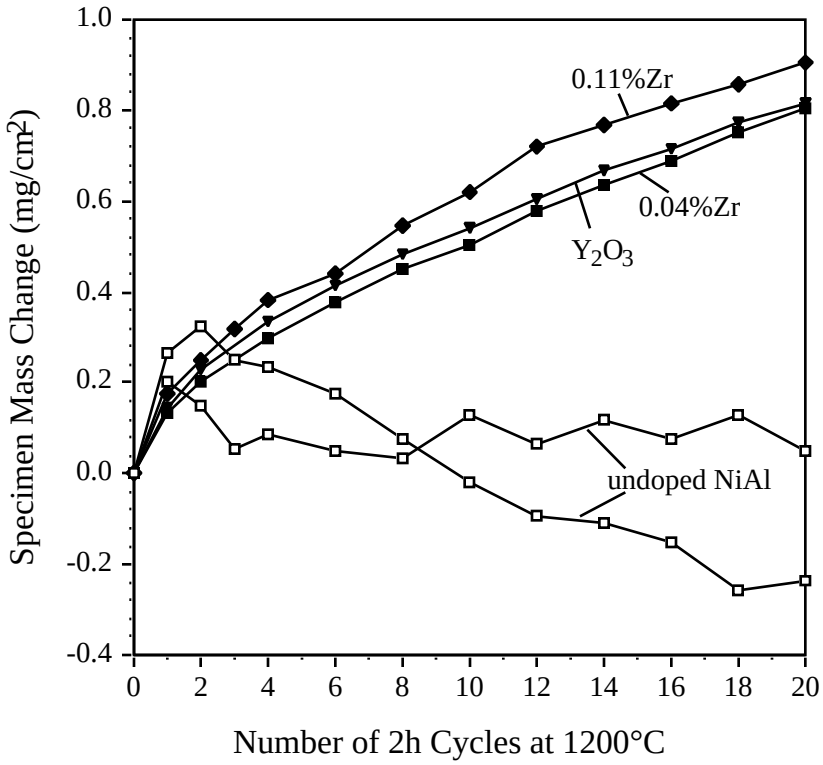

Figure 2. Specimen mass changes during 2h cycles at 1200°C. The three RE-doped alloys showed no scale spallation while mass losses were noted for undoped NiAl.

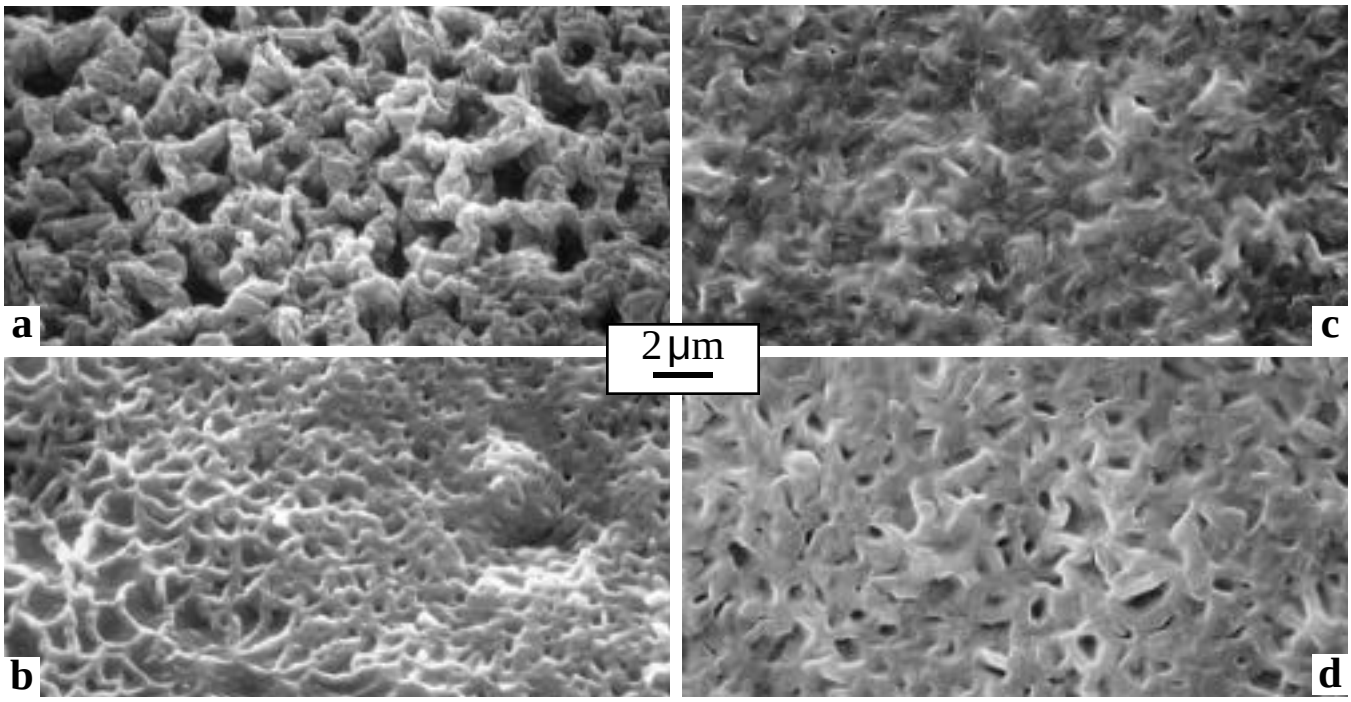

Figure 3. SEM secondary electron plan view images of the scale formed at 1200°C on (a) undoped NiAl after 50h, (b) NiAl+0.11at%Zr after 50h, (c) OD NiAl after 50h and (d) OD NiAl after 200h. The ridges vary from grain to grain (b) but become more distinct on OD NiAl with time, (c) and (d).

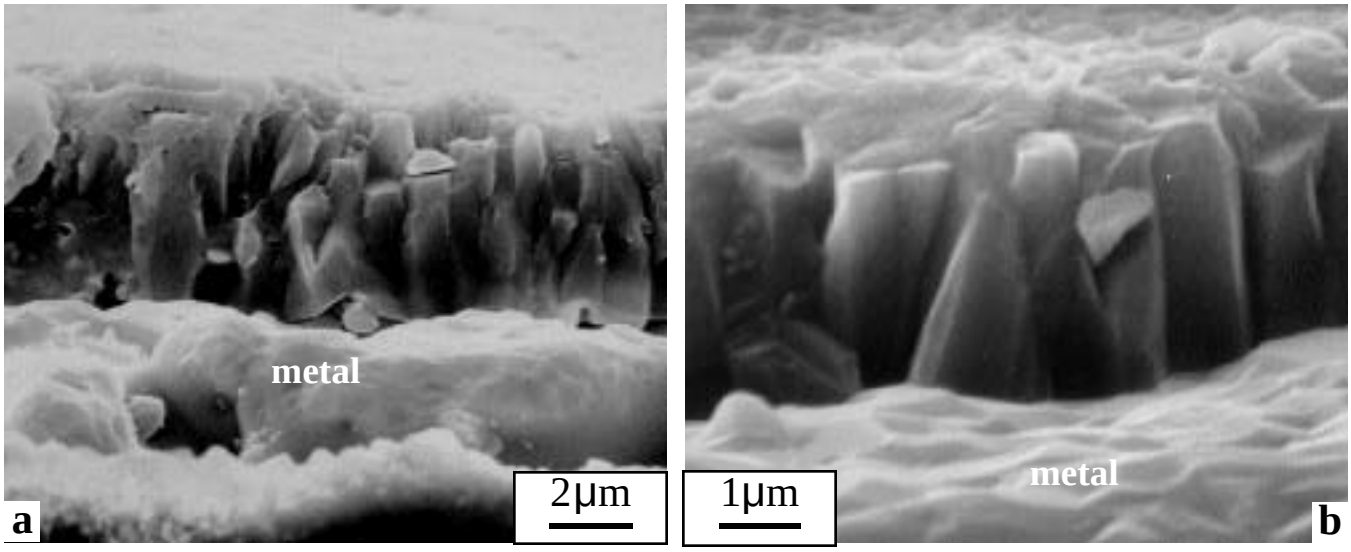

Figure 4. SEM secondary electron cross-sectional images of the scale formed after 50h at 1200°C on (a) OD NiAl and (b) NiAl+0.04at%Zr. Both exhibit a columnar grain structure.

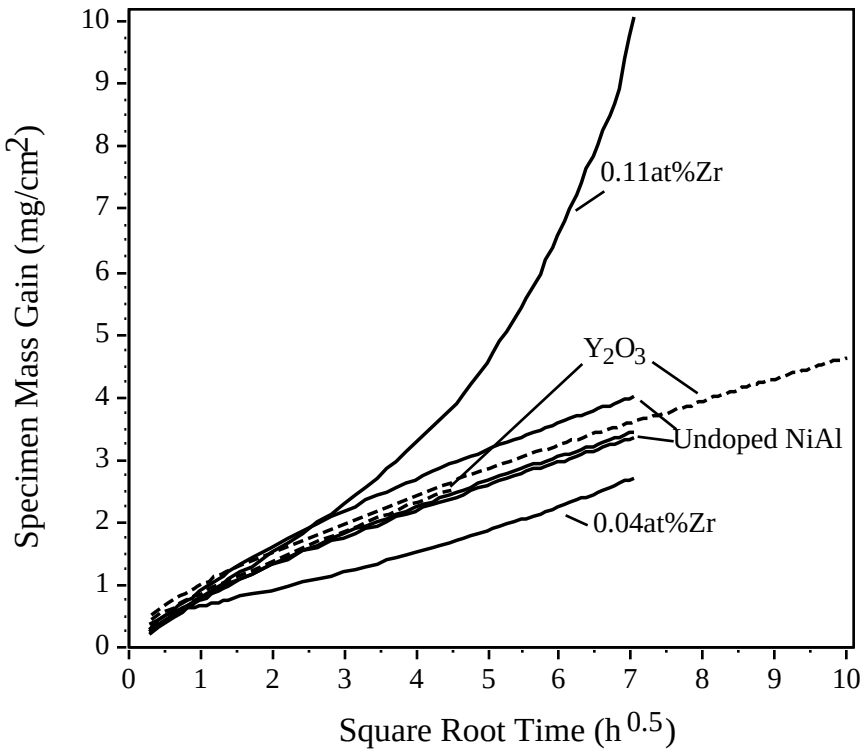

Figure 5. Isothermal oxidation kinetics at 1400°C. At this temperature, the addition of 0.04%Zr or Y_2O_3 has little positive effect. A 0.11at%Zr addition accelerated the oxidation rate compared to undoped NiAl.

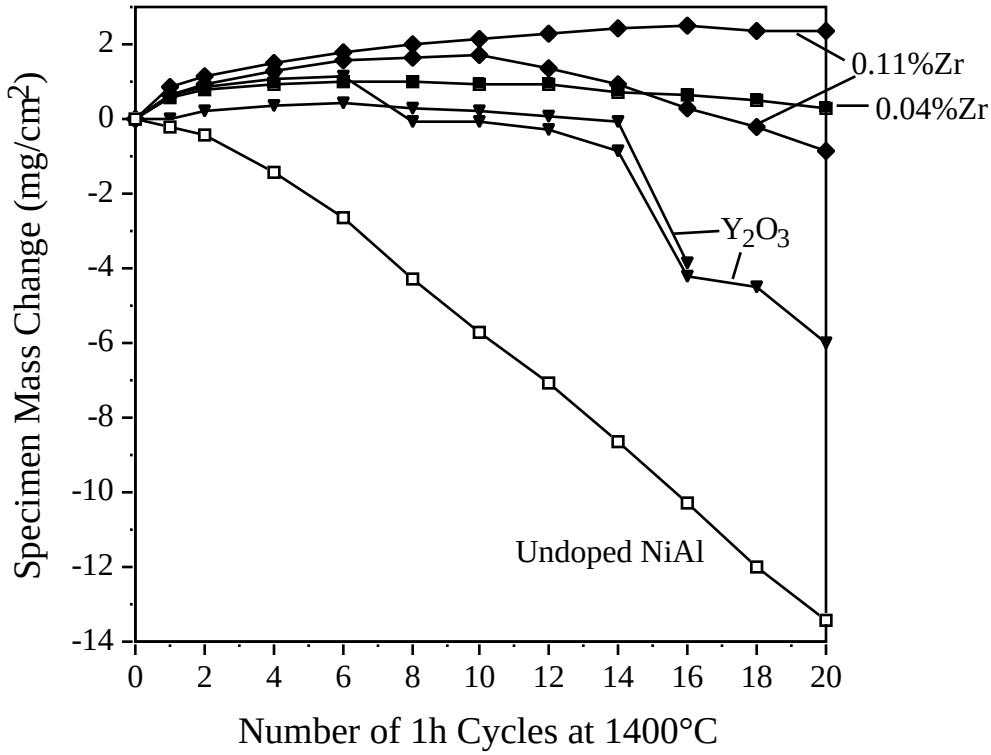

Figure 6. Specimen mass changes during 1h cycles at 1400°C. The three RE-doped alloys showed less mass loss than undoped NiAl, but all had spalled after 20 cycles.

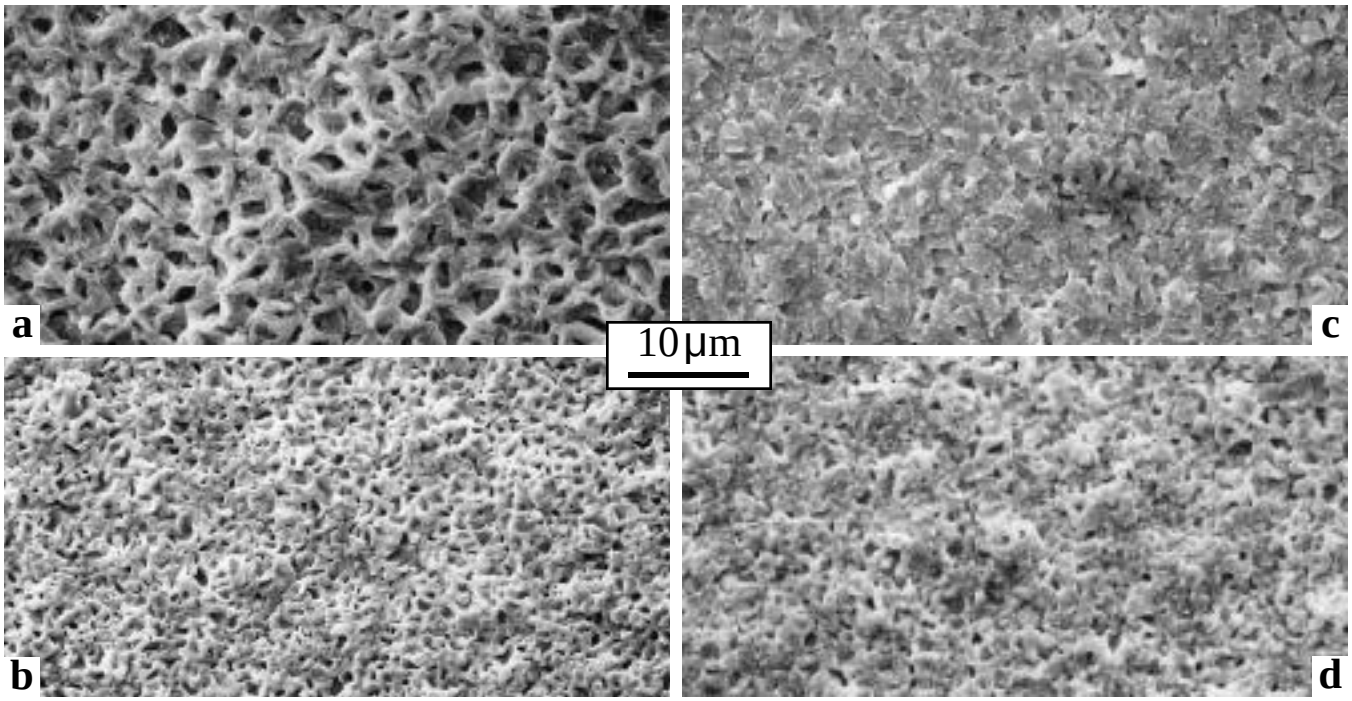

Figure 7. SEM secondary electron plan view images of the scale formed after 1h at 1400°C on (a) undoped NiAl, (b) OD NiAl (c) NiAl+0.04at%Zr and (d) NiAl+0.11at%Zr.

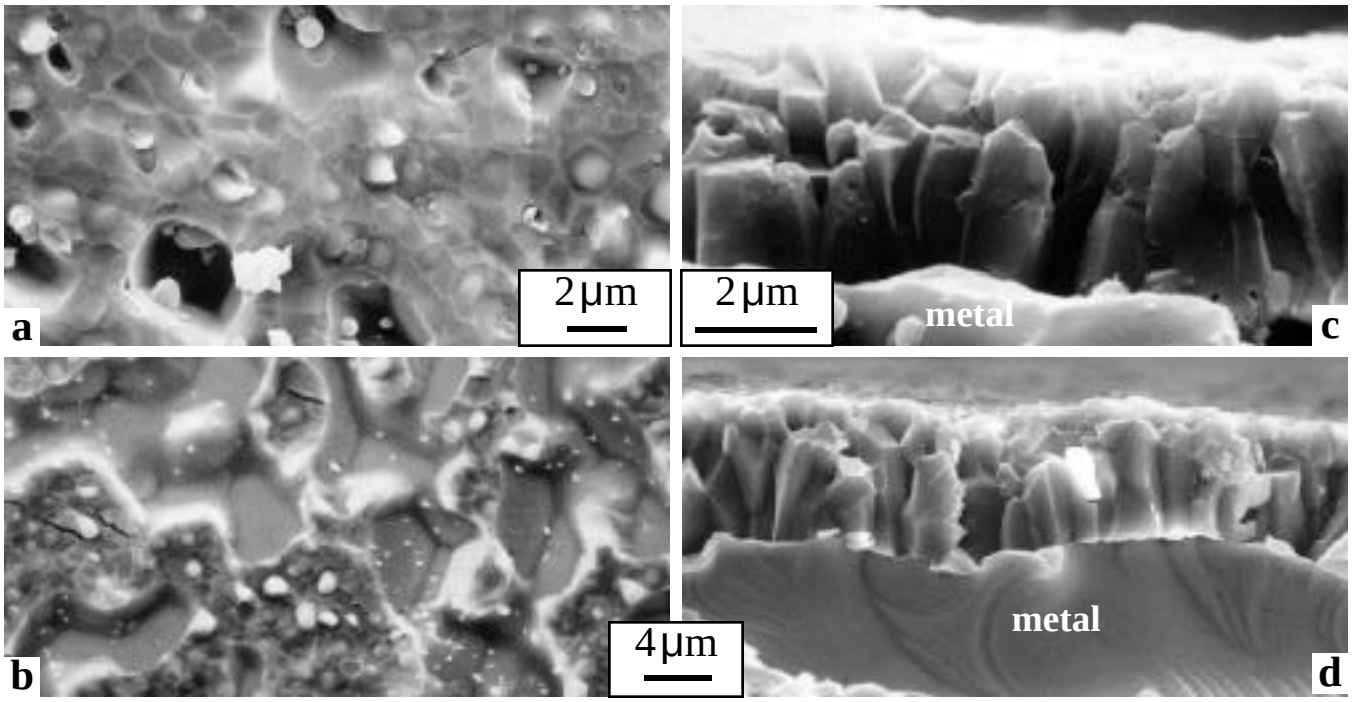

Figure 8. SEM images comparing the metal exposed by scale spallation at 1400°C on (a) OD NiAl after 20, 1h cycles and (b) NiAl+0.11%Zr after 1h and the scale cross-section at the specimen on (c) OD NiAl after 1h and (d) NiAl+0.11%Zr after 10h at 1400°C.

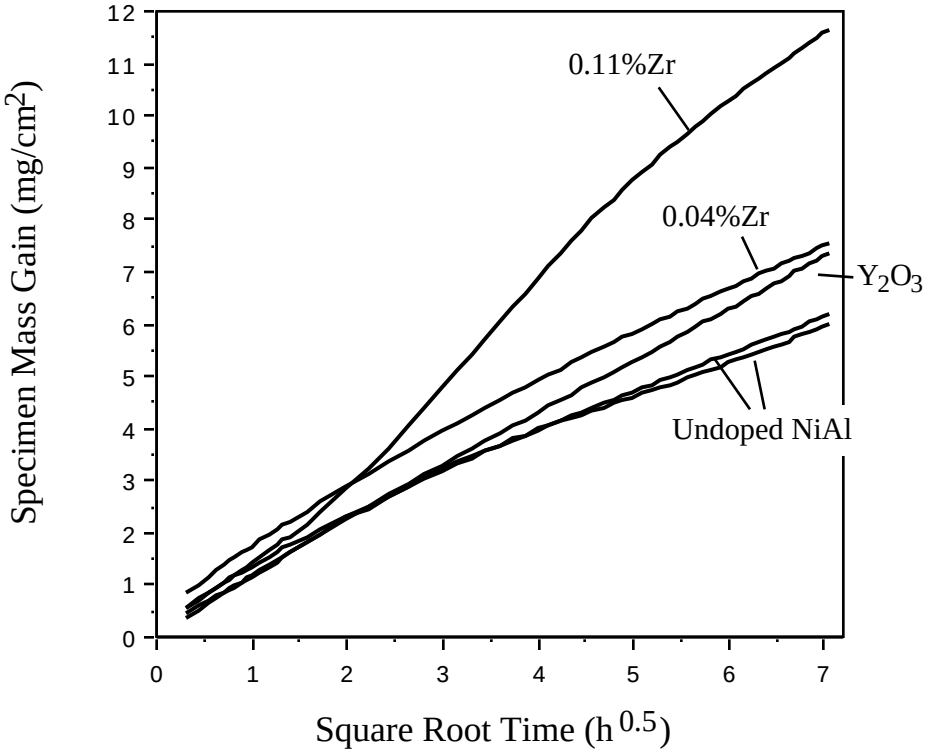

Figure 9. Isothermal oxidation kinetics at 1500°C. Similar to 1400°C, the higher Zr content resulted in accelerated alumina formation.

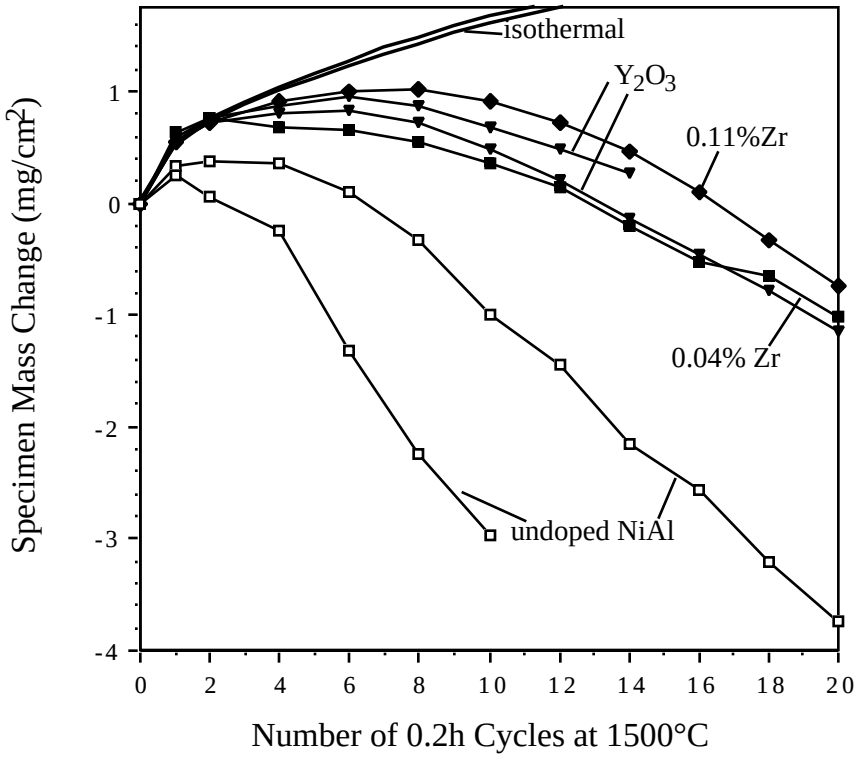

Figure 10. Specimen mass changes during 0.2h cycles at 1500°C. The three RE-doped alloys showed nearly identical behavior with only marginally better scale adhesion than undoped NiAl.

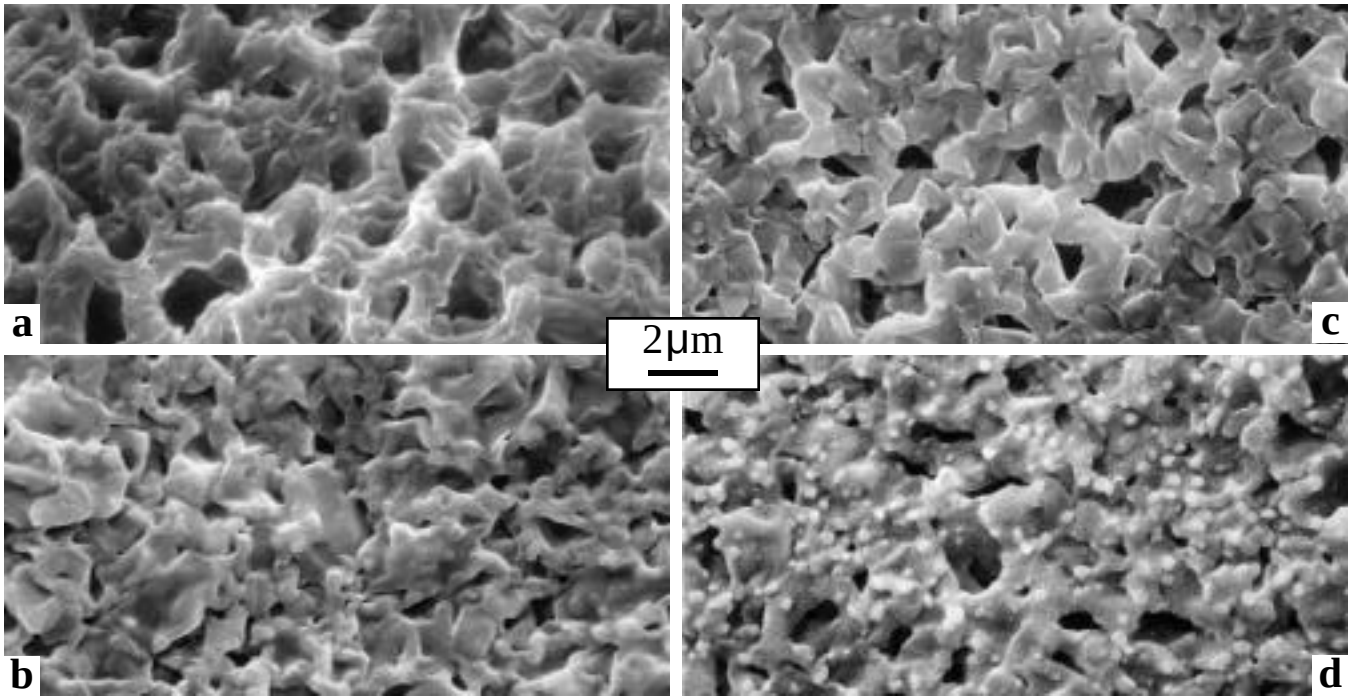

Figure 11. SEM secondary electron plan view images of the scale formed after 0.2h at 1500°C on (a) undoped NiAl, (b) OD NiAl (c) NiAl+0.04at%Zr and (d) NiAl+0.11at%Zr.

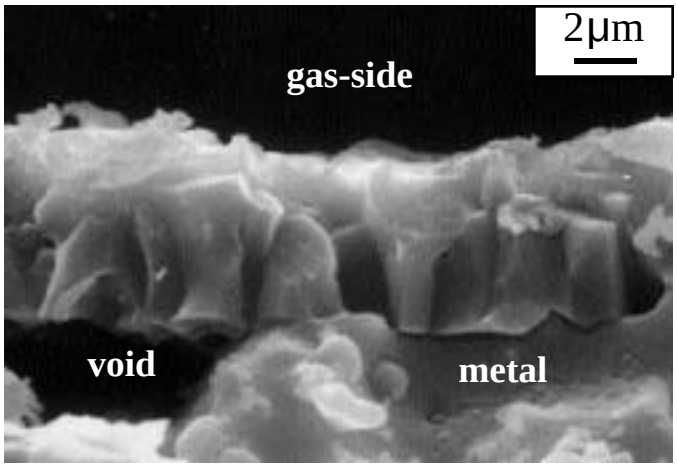

Figure 12. SEM secondary electron image of the specimen edge showing the scale cross-section formed on OD NiAl after 0.2h at 1500°C.

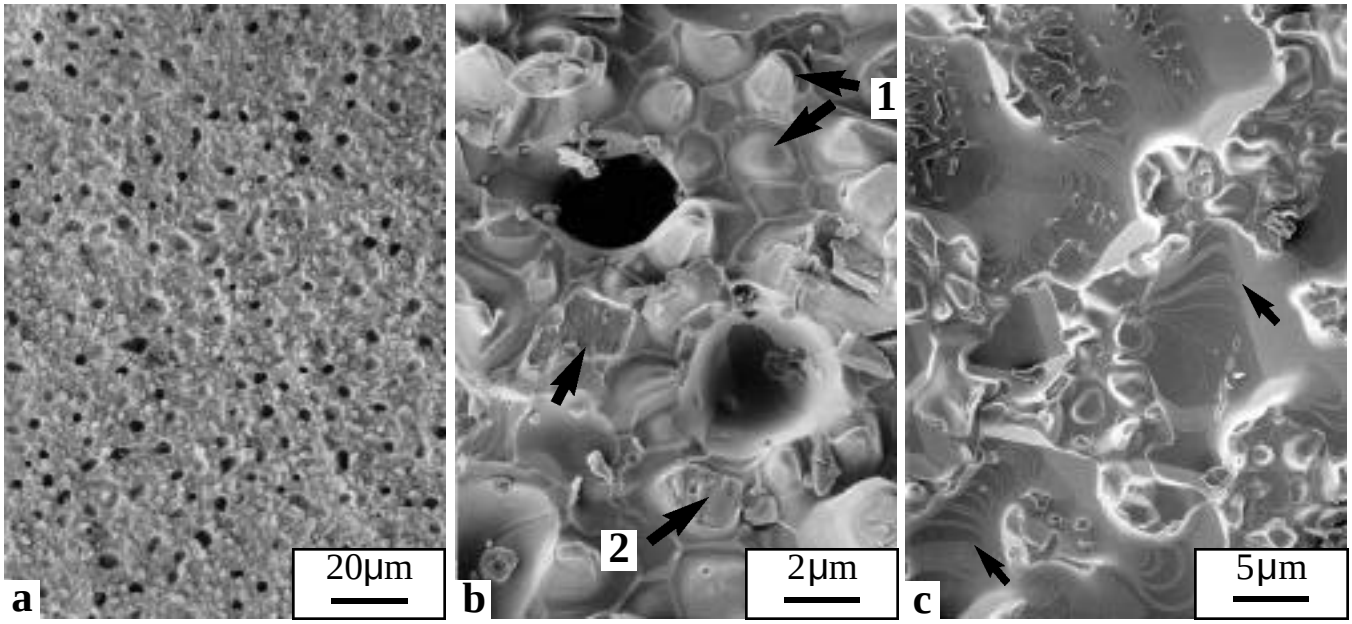

Figure 13. SEM secondary electron plan view images of the metal exposed by scale spallation after 20, 0.2h cycles on (a) and (b) OD NiAl and (c) NiAl+0.04%Zr. Deeper voids were observed in (a) and at higher magnification in (b) on OD NiAl. In (b), #1 arrows mark metal protrusions and #2 arrows mark sheared protrusions. Larger, but shallower voids which showed terracing (arrows) were observed in (c).

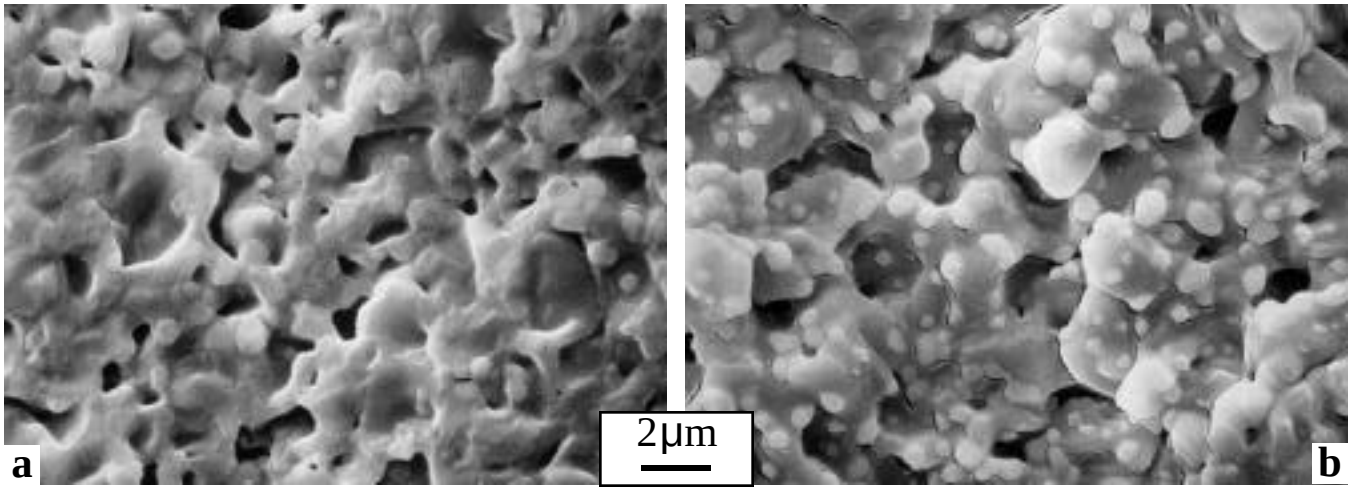

Figure 14. SEM secondary electron plan view images of the scale formed after 4h at 1500°C on (a) OD NiAl and (b) NiAl+0.11at%Zr. The ZrO_2 particles (b) are more prominent than the YAl_xO_y particles (a).